Effect of Carbon Nanotube Functionalization on the Structural and Mechanical Properties of Polypropylene/MWCNT Composites

Anton A. Koval'chuk,*,† Vitaliy G. Shevchenko,‡ Alexander N. Shchegolikhin,§ Polina M. Nedorezova,† Alla N. Klyamkina,† and Alexander M. Aladyshev†

N.N. Semenov Institute of Chemical Physics, Russian Academy of Sciences, Moscow, Russia; N.S. Enikolopov Institute of Synthetic Polymer Materials, Russian Academy of Sciences, Moscow, Russia; and N.M. Emanuel Institute of Biochemical Physics, Russian Academy of Sciences, Moscow, Russia

Received July 16, 2008; Revised Manuscript Received August 22, 2008

ABSTRACT: Multiwall carbon nanotubes (MWCNTs) have been functionalized via addition of undecyl (C_{11}-) radicals generated by thermal decomposition of lauroyl peroxide. The functionalized MWCNTs (C_{11}-MWCNTs) were characterized by Raman, IR spectroscopy, and thermogravimetric analysis (TGA). Isotactic polypropylene (iPP) and syndiotactic polypropylene (sPP) nanocomposites containing both purified and alkyl-functionalized MWCNTs have been synthesized via in situ polymerization method with the use of C_2- and C_s-symmetry zirconocenes activated by MAO in liquid propylene medium. The effect of incorporating C_{11}-MWCNTs on structural, electrical, and mechanical properties of the polypropylene-based nanocomposites has been studied. Analysis of electrical properties in the microwave range elucidates interfacial transformations in the composites induced by MWCNT functionalization and evaluates relative aspect ratios for the filler particles in different systems. The synthesized materials demonstrate improved filler dispersion and mechanical characteristics as a result of nanotube chemical functionalization. The MWCNT functionalization leads to markedly improved nanocomposite plasticity and noticeable enhancement of sPP tensile modulus.

Introduction

Polyolefins (mainly, polypropylene and polyethylene) constitute the family of the most influential and versatile polymer materials of primary commercial importance due to their attractive set of properties and low cost.[1,2] The continuous development of polyolefin-based materials aims at obtaining new properties for achieving further expansion toward new application areas. Great expectations are presently connected with the modification of polymer properties by employing carbon nanotubes (CNTs) as reinforcement filler particles for obtaining novel multifunctional composites combining improved mechanical and thermal properties, electric conductivity, and reduced flammability at low nanotube contents.[3−6] Recent advances in CNT synthesis have enabled their large-scale production with low commercial prices comparable to conventional carbon fibers[7] that opens up possibilities of nanocomposite mass production. However, the problem of CNT aggregation and limited compatibility between nanotubes and polymer matrices, especially polyolefins that have nonpolar chemical structure, makes quite challenging the obtaining polymer composites containing carbon nanotubes. The in situ polymerization approach is regarded in the literature[8−14] as the most promising for efficient CNT dispersion and compatibilization between polyolefins and carbon nanotubes. Metallocene catalysts are the most efficient and versatile tool for obtaining polyolefin-based nanocomposites via in situ polymerization method. Homogeneous metallocenes are soluble in hydrocarbons, and therefore, they can perfectly cover the surface of nanoparticles and fibers.[14,15] Moreover, metallocene catalysts provide unmatched opportunities for the precision synthesis of stereoregular polyolefin architectures and tailoring polymer matrix properties.[16,17]

Recently, we have introduced novel method for obtaining polypropylene/CNT nanocomposites that is appropriate for high-throughput production of the nanocomposites.[18] However, the obtained results have demonstrated that the optimization of the composite interfaces is needed toward achieving enhanced compatibilization between PP matrix and nanotubes and attaining better mechanical performance of the materials. CNT sidewall covalent functionalization is considered as a versatile tool for obtaining improved nanotube dispersion and better compatibility between polymers and nanotubes[19−23] due to the intermolecular interactions between polymer chains and the functional groups grafted to CNTs. In compliance with nonpolar chemical structure of PP macromolecules, attachment of alkyl chains to CNT surface is expected to provide the most efficient interfacial interaction in the respective nanocomposites. In the present work we use the radical mechanism for attaching $-(CH_2)_{10}CH_3$ alkyl chains generated by thermal decomposition of lauroyl peroxide (radical initiator) to multiwall carbon nanotubes (MWCNTs). The MWCNT functionalization has been carried out according to the protocol originally described by Umek et al. for single-wall carbon nanotubes (SWCNTs).[24] The advantage of this chemical functionalization approach over different alkylation methods lies in its simplicity, absence of air- and moisture-sensitive compounds, and high degree of functionalization provided, which makes it suitable for large-scale CNT functionalization.

The effect of MWCNT functionalization on the properties of isotactic (iPP) and syndiotactic polypropylene (sPP) nanocomposites synthesized by in situ polymerization method described in the present paper has not been previously reported in the literature.

Experimental Section

Materials. Pristine CVD-grown MWCNTs (purity ≥95%, average diameter <10 nm, length range 5−15 μm) were purchased from Shenzhen Nanotech Port Co., Ltd., China (trade name of the product is L-MWNTs-10). As-received MWCNTs were purified according to the procedure described elsewhere.[18]

MWCNT chemical functionalization has been carried out in compliance with the following protocol. In a triple-neck flask

* Corresponding author. E-mail: kovalchuk@chph.ras.ru.
† N.N. Semenov Institute of Chemical Physics.
‡ N.S. Enikolopov Institute of Synthetic Polymer Materials.
§ N.M. Emanuel Institute of Biochemical Physics.

10.1021/ma801599q CCC: $40.75
Published on Web 09/24/2008

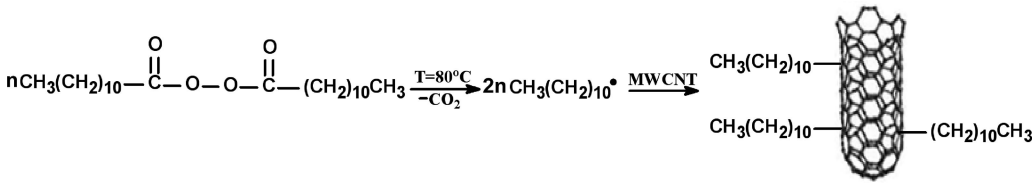

Figure 1. Reaction scheme of MWCNT functionalization.

(volume 1.0 L) equipped with a magnetic stirrer, external heater, control thermocouple, and condenser, 2.0 g of purified and vacuum-dried MWCNTs was dispersed by magnetic stirring in 900 mL of toluene under argon, and 2.0 g of lauroyl peroxide (95%, purchased from Acros) was added. Temperature has been raised to 80 °C. Next, 2.0 g portions of lauroyl peroxide have been added upon finishing every 60 min of synthesis. Total reaction time was 15 h, and overall weight of consumed lauroyl peroxide was 30 g. The obtained undecyl-functionalized MWCNTs (C_{11}-MWCNTs) were filtered and repeatedly washed with toluene and heptane, finally dried in a vacuum at 130 °C for 3 h, and then stored in an argon atmosphere.

Polymerization grade propylene was provided by Moscow Oil Refining Plant and used in nanocomposite synthesis without any additional treatment. Isospecific C_2-symmetry metallocene catalyst *rac*-Me_2Si(2-Me-4-PhInd)$_2ZrCl_2$ (MC-1) for iPP/MWCNT and iPP/C_{11}-MWCNT nanocomposite preparation was purchased from Boulder Scientific Co., and C_s-symmetry metallocene Ph_2C(Cp)-FluZrCl_2 (MC-2) for obtaining sPP/MWCNT and sPP/C_{11}-MWCNT nanocomposites was synthesized in Moscow State University according to the technique described in the literature.[25] MAO as a 10 wt % solution in toluene has been purchased from Witco and used as received. Metallocenes were used in a form of toluene solutions (0.01−0.03 wt %) preactivated with MAO. Polymerization experiments were carried out at 60 °C temperature and 2.5 MPa pressure in a 200 cm^3 stainless steel autoclave reactor equipped with an internal sonotrode for MWCNT ultrasonication and a high-speed mechanical stirrer (3000 rpm). The reactor, containing required amount of MWCNTs, was evacuated for 1.5 h at 60 °C before polymerization experiments and then filled with 150 mL of liquid propylene and 2.5−5 g of 10 wt % MAO solution. The prereaction mixture was sonicated then for 30 min with the use of 300 W 40 kHz ultrasonic generator with additional mechanical stirring. Polymerization assisted by mechanical stirring has been started immediately after MWCNT ultrasonication by injecting metallocene solution into the precooled (10 °C for MC-1/MAO or 20 °C for MC-2/MAO) reactor to provide homogeneous distribution of active sites on MWCNT surface. After a 2 min initial stage of polymerization the reaction temperature has been raised to 60 °C. Polymerizations were carried out for 10−19 min (for iPP composites) or 9−35 min (for sPP materials) and then quenched by adding ethanol. After polymerization, the composite powder was extracted from the reaction mixture by simple depressurizing the unreacted propylene gas from the reactor.

Composition of the materials was controlled by adjusting three variables, namely MWCNT (or C_{11}-MWCNT) weight, polymerization time, and metallocene amount. Catalyst amounts ranged between 3.0×10^{-7} and 4.6×10^{-7} mol for MC-1 and between 1.1×10^{-6} and 2.3×10^{-6} mol for MC-2. The MAO/zirconium molar ratio has been kept within the bounds of 12 000−14 000 for MC-1/MAO catalyst system and 4500−7000 for MC-2/MAO.

After polymerization quenching, the composites were placed for 24 h in ethanol acidified by hydrochloric acid in order to remove aluminum hydroxide and catalyst residues. After that, the materials have been repeatedly washed with distilled water and ethanol and then dried in a vacuum at 40 °C.

Characterization. Raman spectra of MWCNTs and C_{11}-MWCNTs have been acquired with the aid of a Senterra Raman microscope (Bruker) furnished with a 785 nm laser excitation. The Raman spectra of the MWCNTs and C_{11}-MWCNTs were run at comparatively low excitation powers in the range 1−10 mW. While such excitation powers are quite adequate for obtaining a resonantly enhanced Raman spectrum of MWCNTs with good signal-to-noise ratio, they are not sufficient to excite strong spontaneous (nonresonant) Raman spectrum of aliphatic C_{11}-chains. FT-IR measurements of MWCNTs and C_{11}-MWCNTs were conducted on a Vertex 70 FT-IR spectrometer (Bruker). Intrinsically, useful IR transmission spectra of CNTs in KBr matrix can be obtained only at very high KBr/CNT dilution ratios (usually in the range of 300/1−500/1). Inevitably, KBr contributes its own spectral features (originating mainly from entrapped water) in the resulting spectrum, and these can be overwhelmingly intense at the high dilution ratios. That is why, to extract and enhance the spectral features belonging to the MWCNTs, we employed careful digital subtraction of the KBr matrix contribution from the as-measured MWCNT/KBr disk spectra.

TGA data of MWCNT and C_{11}-MWCNT samples were collected in an argon atmosphere on a TG 209 F1 instrument (Netzsch), with a heating rate of 10 K/min.

Molecular weights and molecular weight distributions of the neat polymers were evaluated by GPC in a Waters 150C at 130 °C by using linear μ-styragel HT columns and 1,2,4-trichlorobenzene as the eluent. The molecular weights were determined by employing polystyrene calibration curve as a reference.

The uniaxial tensile testing of the nanocomposites has been performed at room temperature (20 °C) on an Instron 1122 machine at 50 mm/min tensile speed. The film samples for mechanical testing were prepared by hot pressing of the nanocomposite powders at 190 °C and 10 MPa for 5 min and subsequent cooling at 16 K/min rate, and dog-bone specimens (with dimensions $35 \times 5 \times 0.5$ mm) have been cut from films. Multiple tests (five for each material) have been implemented for the reproducibility.

The gross dispersion of MWCNT bundles was observed using optical microscopy on hot-pressed nanocomposite films of 80 μm in thickness by employing a Carl Zeiss transmission light microscope equipped with a CCD camera. Morphology of fracture surfaces of the nanocomposite films has been observed by using a Hitachi S-520 scanning electron microscope (SEM). Isotropic film samples (0.5 mm thick) prepared as mentioned above were fractured in liquid nitrogen and gold-sputtered prior to SEM imaging. Transmission electron microscopy (TEM) observations of the nanocomposites were performed on a LEO-912AB transmission electron microscope. Analyzed samples were prepared by cutting melt-pressed films to ~100 nm thick slices using a Reichert-Jung Ultracut microtome.

The dc conductivity of the materials was measured by utilizing a two-probe method at room temperature for the film samples (0.5 mm thick). Electrical properties of the polypropylene/MWCNT nanocomposite films in microwave range (3.2−40 GHz) have been evaluated by the cavity resonance method using KSVN R-2 instruments (Russia) with rectangular-shaped resonators (H0ln operating mode). The cavity resonance method is based on the determination of resonance frequency change Δf and the change of cavity Q factor $(1/Q - 1/Q_0)$ when the measured sample is inserted into the cavity. Direct measurements yield real (ε') and imaginary (ε'') parts of nanocomposite permittivity.

Results and Discussion

MWCNT Functionalization. The reaction sequence corresponding to MWCNT functionalization is depicted in Figure 1. The efficient MWCNT sidewall functionalization by thermal

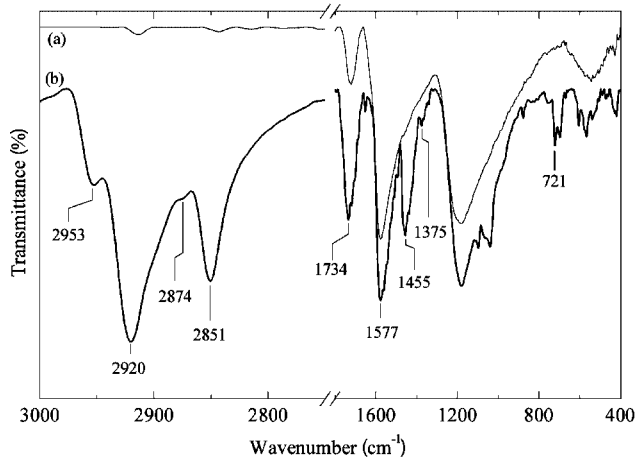

Figure 2. FTIR spectra of purified MWCNTs (a) and of C_{11}-MWCNTs (b). The spectra are normalized by the MWCNT phonon band intensity (1577 cm^{-1}) and are offset along the ordinate for clarity. The vibrational modes that emerged as the result of MWCNT functionalization are CH_3 antisymmetric stretch (2953 cm^{-1}), CH_2 antisymmetric stretch (2920 cm^{-1}), CH_3 symmetric stretch (2874 cm^{-1}), CH_2 symmetric stretch (2851 cm^{-1}), CH_3 antisymmetric bend + CH_2 "scissors" bend (1455 cm^{-1}), CH_3 symmetric bend (1375 cm^{-1}), and concerted rocking of the $(CH_2)_n$ chain (721 cm^{-1}).

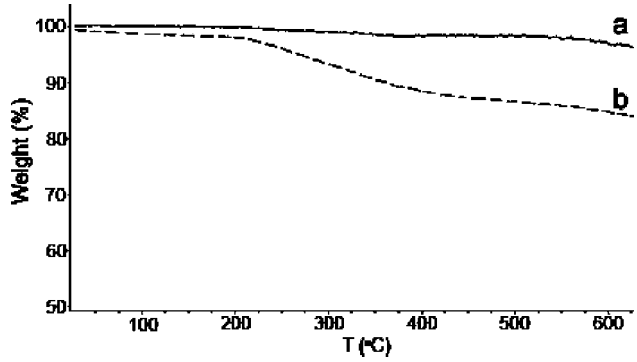

Figure 3. TGA profiles of purified MWCNTs (a) and C_{11}-MWCNTs (b).

decomposition of lauryl peroxide has been confirmed with the aid of complete (FTIR + Raman) vibrational spectra. According to Raman spectra (see Supporting Information), the disorder band intensity (D peak) has increased notably for C_{11}-MWCNTs as compared to that of purified MWCNTs. Accordingly, not taking into account the observed G/D bands intensity redistribution, the Raman spectra are actually devoid of features directly, confirming successful functionalization of MWCNT with the C_{11}-pendants. On the contrary, FTIR spectra are capable of providing a plenty of convincing information about the aliphatic chains. Figure 2 shows the resultant FTIR spectra for MWCNT and C_{11}-MWCNT after KBr contribution subtraction. The successful functionalization of the MWCNTs with undecyl radicals is unambiguously confirmed by emergence in the C_{11}-MWCNT spectrum of the following series of vibrational bands: 2953 cm^{-1} (CH_3 antisymmetric stretch), 2920 cm^{-1} (CH_2 antisymmetric stretch), 2874 cm^{-1} (CH_3 symmetric stretch), 2851 cm^{-1} (CH_2 symmetric stretch), 1455 cm^{-1} (CH_3 antisymmetric bend + CH_2 "scissors" bend), 1375 cm^{-1} (CH_3 symmetric bend), and 721 cm^{-1} (concerted rocking of the $(CH_2)_n$ chain).

The TGA profile of derivatized MWCNTs demonstrates considerable weight loss in the temperature range 200−500 °C (Figure 3) which corresponds to the thermal disruption of the alkyl attachments. According to the TGA, the high degree of MWCNT functionalization has been achieved: C_{11}-MWCNTs contain nearly 10 wt % of $-(CH_2)_{10}CH_3$ groups. It should be mentioned that comparable functionalization degrees have been reported earlier for MWCNTs derivatized through the Billups reaction,[26] but the current functionalization protocol is more feasible for a large-scale realization since it requires less complicated reaction conditions and is more environmentally appropriate.

Nanocomposite Synthesis Results. Four series of iPP- and sPP-based nanocomposites containing both purified and functionalized MWCNTs with filler loadings ranging from 0.1 to 3.6 wt % have been obtained by the in situ polymerization method in liquid propylene medium.

According to the composite synthesis peculiarities, metallocene active sites are assumed to be partly heterogenized on the nanotube surface and partly distributed in solution in the homogeneous state. Nevertheless, the composite powder examination provides clear evidence of efficient catalyst heterogenization achieved by propylene in situ polymerization: homogeneous grayish powders without visible traces of pure iPP or sPP have been obtained, and noticeable reduction of the reactor fouling (which takes place in the absence of filler) was observed. Prevention of reactor fouling in presence of nanofiller has also been reported by Mulhaupt et al. for PE/boehmite nanocomposites prepared by in situ polymerization.[27] For iPP-based nanocomposites, dramatic transformation in powder morphology as compared to the neat iPP has been observed. Unlike gross grainy powders of the neat iPP (average diameter of grains is ~0.5 mm), iPP/MWCNT and iPP/C_{11}-MWCNT nanocomposite powders consist of very small fibril-like particles of submillimeter diameter. Bulk density considerably decreases from ~0.25 g/cm^3 for the neat iPP to ~0.07−0.09 g/cm^3 for the iPP composite powders. Nevertheless, sPP-based composites do not exhibit transformation in powder morphology in comparison with the pure sPP (fine-grained powders have been obtained in all the experiments), and only color change from white to progressive gray depending on filler content takes place.

Catalyst activity remains almost unchanged in presence of MWCNTs or C_{11}-MWCNTs either for MC-1/MAO (~90−100 kg iPP/(mmol Zr h)) or for MC-2/MAO (~25−30 kg sPP/(mmol Zr h)). Constancy of catalyst activity enables precision control of filler content in the composites.

Molecular weight of the neat iPP synthesized in the identical conditions to the nanocomposites is $M_w \sim 600\,000$ ($M_w/M_n = 2.2$), and of the neat sPP is ~310 000 ($M_w/M_n = 2.0$).

Microstructure of the Nanocomposites. Optical and scanning electron microscopy observations clearly demonstrate that the MWCNT functionalization leads to better filler dispersion on both micro- and nanoscale in iPP and sPP matrices. Figure 4 illustrates that the nanotube alkylation notably facilitates the decrease of filler aggregate size, since the attachment of functional groups to MWCNT surface promotes repulsion forces between the modified nanotubes. Thus, originally achieved fair MWCNT distribution has been distinctly improved by the functionalization, and we can state that CNT chemical modification is very important for attaining well nanotube dispersion in the nanocomposites.

SEM imaging clarifies a considerable difference between various composite systems in nanotube dispersion efficiency achieved in polymer matrices (Figure 5). Originally, a high exfoliation degree of nanotube aggregates has been attained in iPP/MWCNT nanocomposites (Figure 5a): well-separated individual MWCNTs prevail in a filler phase that is result of powerful prepolymerization sonication. However, the composite fracture surfaces reveal evident nanotube pull-out, indicating low interfacial interaction between the PP matrix and MWCNTs. According to the morphology of the nanocomposite fracture surfaces, MWCNT chemical functionalization provides com-

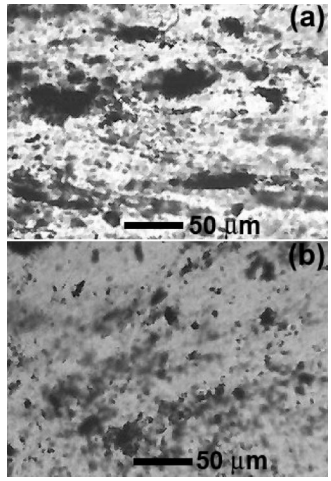

Figure 4. Transmission light microscopy images of iPP/0.4 wt % MWCNT (a) and iPP/0.4 wt % C_{11}-MWCNT (b) nanocomposite thin films.

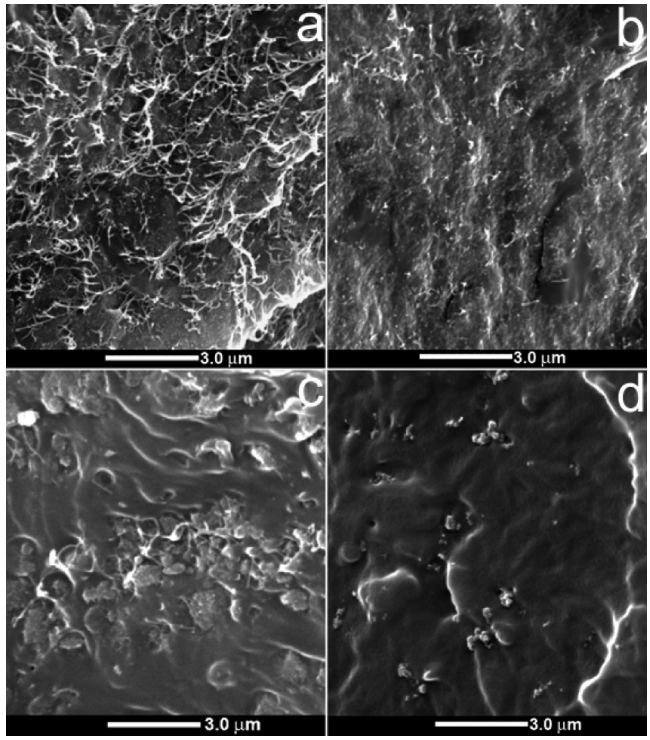

Figure 5. SEM images of the iPP and sPP nanocomposites: iPP/1.4 wt % MWCNT (a), iPP/1.2 wt % C_{11}-MWCNT (b), sPP/1.5 wt % MWCNT (c), and sPP/1.5 wt % C_{11}-MWCNT (d).

patibilization between the modified nanotubes and polymer matrix, since nanotube pull-out becomes not prominent (Figure 5b), that shows higher interaction between the polymer and C_{11}-MWCNT in comparison with MWCNTs. Certain improvement in the MWCNT dispersion on the nanoscale has also been observed upon the functionalization. TEM images presented in the Supporting Information illustrate this improvement.

While well-separated individual MWCNTs are predominant in iPP/MWCNT materials, sPP-based composites exhibit strong filler aggregation. For the sPP/0.4 wt % MWCNT sample, prevalent formation of relatively compact nanotube clusters integrating 6−8 individual nanotubes takes place, but at filler contents higher than 1.5 wt % strongly agglomerated CNT structures with micrometer dimensions are formed in the sPP matrix (Figure 5c). These microstructural features of the composites have a strong connection with the materials properties that will be discussed below. Because of the considerable nanotube aggregation, the sPP/MWCNT materials have substantially lower interfacial area as compared to the iPP/MWCNT nanocomposites that especially correlates with the electrophysical properties of the composites. We suppose that the filler aggregation in the sPP/MWCNT composites is mostly related to the catalytic aspect of in situ polymerization. The previous studies on propylene polymerization kinetics conducted in comparable experimental conditions demonstrated that the rate of MC-2/MAO active sites formation is considerably lower in comparison with MC-1/MAO.[28,29] Thus, it is assumed that the coating of filler particles with polymer shells is delayed for the sPP/MWCNT composites as compared to the iPP/MWCNT, and nanotubes have much more freedom to reaggregate in the presence of MC-2 catalyst. Consequently, the catalytic peculiarities of in situ polymerization not only determine the productivity of composite synthesis and polymer matrix properties but also have a strong influence on nanotube dispersion. The fact of this strong MWCNT aggregation in the sPP composites demonstrates a great problem of dispersing small-diameter nanotubes with a high aspect ratio in nonpolar hydrocarbon solvents that cannot be resolved even by combining intense ultrasonication and high-speed (3000 rpm) mechanical stirring. The chemical functionalization has a crucial role in enabling nanotube exfoliation in sPP-based composites prepared via the in situ polymerization method by utilizing the MC-2/MAO catalyst system. Thus, upon incorporating C_{11}-MWCNTs in the sPP matrix, the notable reduction of an average nanotube aggregate size has been observed (Figure 5d) which is a result of improved MWCNT suspension stability. The considerable increase in interfacial area for the sPP/C_{11}-MWCNT composites as compared to the sPP/MWCNT has also been confirmed by the microwave electrical measurements which provide bulk characterization of the materials.

Electrical Properties. The percolation transition has not been detected by DC measurements in the iPP-based and sPP-based composites containing both MWCNTs and C_{11}-MWCNTs in the studied filler concentration range (up to 3.6 wt %). This behavior can be explained by perfect encapsulation of filler particles with polymer shells achieved via the in situ polymerization method which impedes formation of conductive paths in the iPP-based nanocomposites. For the sPP composites, imperfect exfoliation of MWCNT agglomerates is the most probable explanation for this fact. Anyway, it is consistent with the existing literature data for polyolefin/MWCNT composites[30−32] for those percolation thresholds at ∼8 wt % filler concentration are reported.

Analysis of electrical properties of the nanocomposites in a microwave range provides deep insight into the microstructural features of the synthesized materials. Microwave measurements demonstrate differences in the electrical properties between the composites containing purified and functionalized MWCNTs revealing structural transformations in the materials caused by the nanotube functionalization. The angle of slope of the near-linear dependences between the nanocomposite permittivity and filler concentration (Figure 6) is increased for the composites filled with C_{11}-MWCNTs. The slope of the respective line depends on the depolarization coefficient of filler particles, which is determined by the aspect ratio (l/d) of nanotubes. These functional dependences have been analyzed with the use of the mathematical model derived from Bruggeman's equation described earlier.[18,33] According to the corresponding calculations, the relative average aspect ratio for nanotubes increases from ∼25 for iPP/MWCNT to ∼32 for the iPP/C_{11}-MWCNT system and from ∼10 for sPP/MWCNT to ∼19 for sPP/C_{11}-MWCNT. The given values do not correspond to the actual nanotube aspect ratios in the investigated composites and only allow us to make

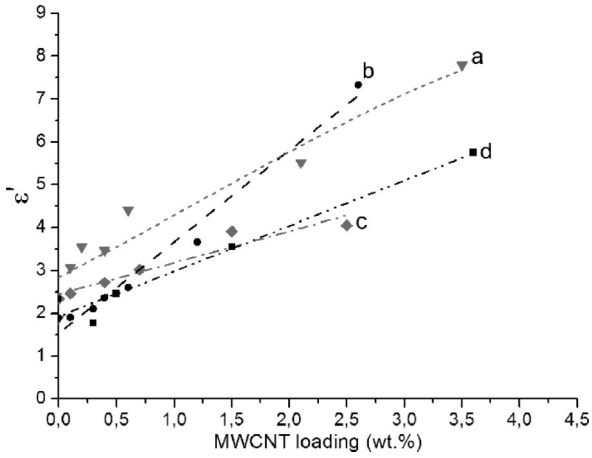

Figure 6. Permittivity at 4.8 GHz frequency as a function of filler loading for iPP/MWCNT (a), iPP/C_{11}-MWCNT (b), sPP/MWCNT (c), and sPP/C_{11}-MWCNT (d) nanocomposites.

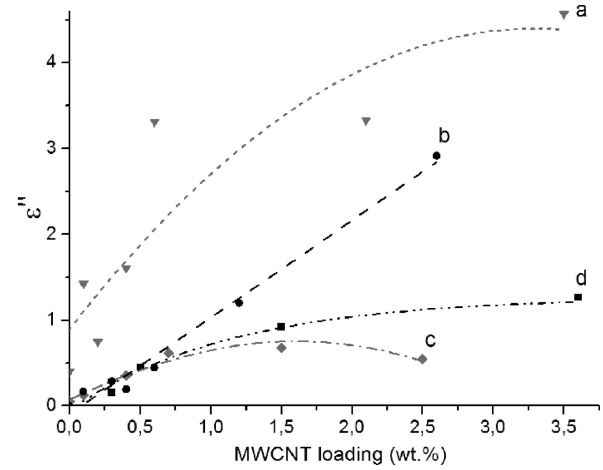

Figure 7. Correlation between dielectric losses (ε'') and nanotube loading for iPP/MWCNT (a), iPP/C_{11}-MWCNT (b), sPP/MWCNT (c), and sPP/C_{11}-MWCNT (d) nanocomposites at 3.2 GHz frequency.

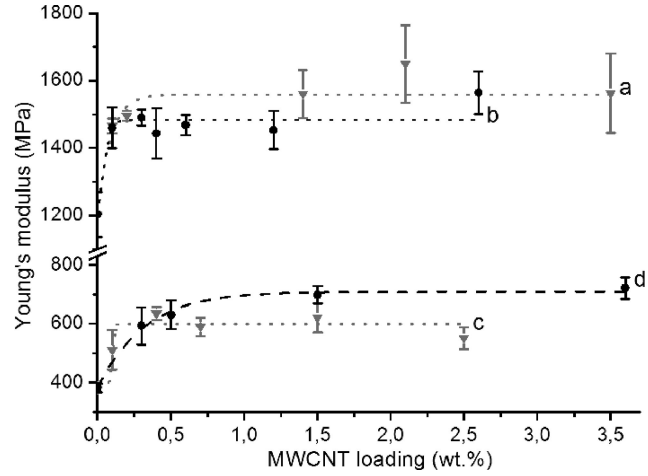

Figure 8. Young's modulus of iPP/MWCNT (a), iPP/C_{11}-MWCNT (b), sPP/MWCNT (c), and sPP/C_{11}-MWCNT (d) nanocomposites as a function of MWCNT loading.

approximate comparison of MWCNT anisotropy coefficients in different composite systems. These results demonstrate considerable improvement in the MWCNT dispersion efficiency achieved by the chemical functionalization for the sPP-based composites. In other words, functionalized nanotubes more fully exhibit their "native" aspect ratio in composite material. Thus, microwave electrical analysis provides convenient solution for studying nanotube aggregation in various polymer composite systems.

Incorporation of MWCNTs in iPP or sPP imparts electromagnetic absorbance properties to the polymers. The increased aspect ratio in combination with the method of synthesis preventing electrical contacts between individual nanotubes makes these materials suitable for effective absorption of electromagnetic radiation. Indeed, as was found in ref 33, composites with short carbon fibers (aspect ratio ~80) exhibit rapid nonlinear increase of permittivity with increased loading, while for similar fibers, coated with dielectric layer, which prevented electrical contacts between them, this dependence was linear (as in our case for MWCNTs) and the composite showed good absorbing properties. A similar effect was observed by Thomassin et al.[34] when the reflectivity of nanocomposites containing carbon nanotubes decreased upon foaming the matrix. In this case foaming leads to separation of individual nanotubes and loss of electrical contacts between them, resulting in lower bulk conductivity of the material. These foamed MWCNT nanocomposites are superior because their performance results from absorption at low filler content and not from reflection at relatively high filler content as in solid material. The same effect is brought about by the method of in situ polymerization for the PP/MWCNT composites. Considerable dielectric losses (electromagnetic energy dissipation) within the iPP/MWCNT nanocomposites have been detected in a microwave range (Figure 7a). The sPP/MWCNT composites displayed notably reduced electromagnetic energy dissipation (Figure 7c) as a result of much lower interfacial area that has been discussed above. The better nanotube dispersion in the sPP/C_{11}-MWCNT materials caused by the chemical functionalization improves electromagnetic absorbance properties of the composites (Figure 7d). The iPP/C_{11}-MWCNT nanocomposites, however, exhibit some reduction in dielectric losses in comparison with the iPP/MWCNT materials (Figure 7b) despite the improved nanotube dispersion. This fact can be attributed to the distortion of the nanotube π conjugated electronic structure caused by the chemical functionalization that leads to sacrificing microwave absorbance properties of the composites. Nevertheless, the iPP/C_{11}-MWCNT nanocomposites retain high electromagnetic energy dissipation properties and can be considered as promising materials for the EMI shielding and electromagnetic absorbance applications.

Mechanical Properties. Tensile experiments demonstrate that noticeable mechanical reinforcement effect is observed in the iPP and sPP composites even upon incorporating lowest nanotube amount: at 0.1 wt % MWCNT loading Young's modulus of iPP increases by ~22% from ~1200 to ~1465 MPa, and modulus of sPP grows by ~34% from ~380 to ~510 MPa (Figure 8). Subsequent modulus enhancement continues up at higher filler concentrations. Ultimate Young's modulus improvement of iPP is ~37% (from ~1200 to ~1650 MPa) at 2.1 wt % MWCNT content. For the sPP/MWCNT composites maximal mechanical reinforcement is achieved at 0.4 wt % nanotube loading (Young's modulus grows by ~66% from ~380 to ~635 MPa), and posterior modulus reduction at higher nanotube contents signifies considerable impact of MWCNT aggregation that takes place in this system. Generally, all the studied systems exhibit higher modulus increment at low MWCNT concentrations (below 1 wt %) at which the maximal aspect ratios for the filler particles are attained. (A plateau in modulus dependence is reached for nanotube concentration of roughly 0.5 wt % for all types of composites tested, except for sPP/C_{11}-MWCNT, where the plateau is reached at ca. 1.5 wt %.) The incorporation of C_{11}-MWCNTs in iPP matrix produces the same reinforcing effect as compared to MWCNTs (~30%

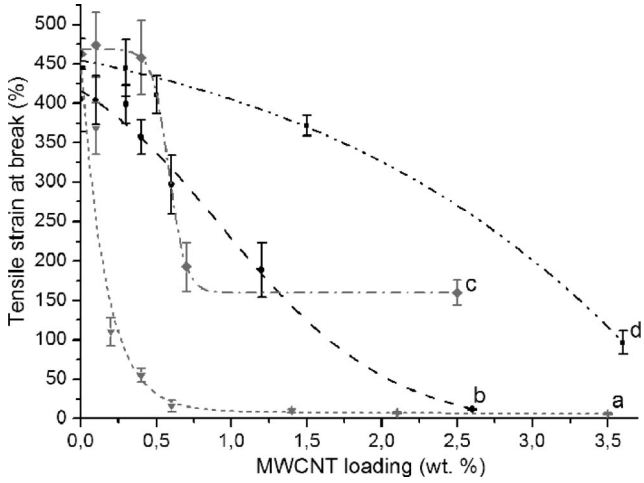

Figure 9. Strain at break values of iPP/MWCNT (a), iPP/C_{11}-MWCNT (b), sPP/MWCNT (c), and sPP/C_{11}-MWCNT (d) nanocomposites corresponding to the different filler loadings.

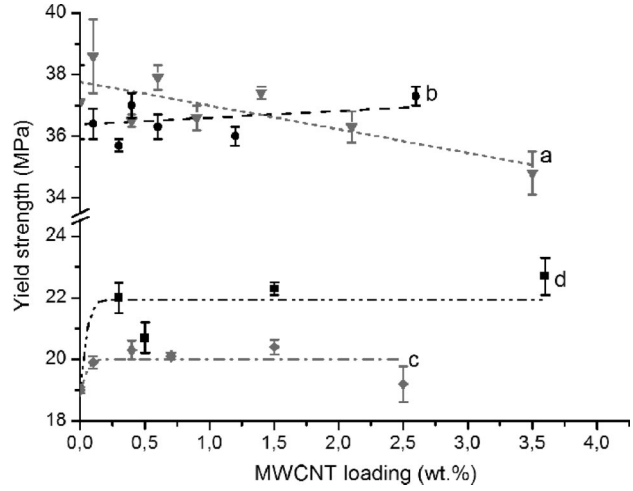

Figure 10. Correlations between the yield strength and filler content for iPP/MWCNT (a), iPP/C_{11}-MWCNT (b), sPP/MWCNT (c), and sPP/C_{11}-MWCNT (d) nanocomposites.

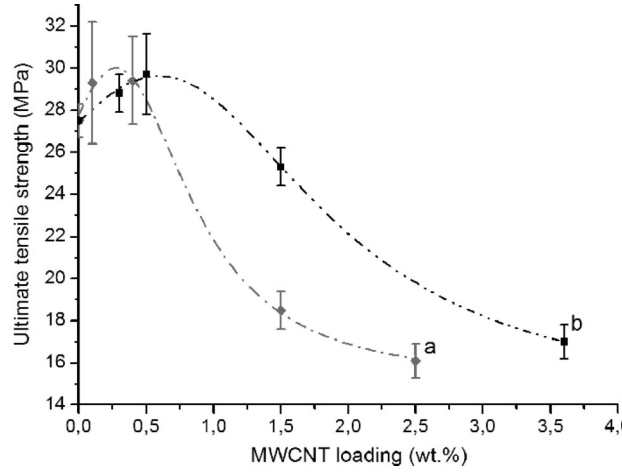

Figure 11. Tensile strength at break for the sPP/MWCNT (a) and sPP/C_{11}-MWCNT (b) composites at different filler concentrations.

improvement in Young's modulus at 2.6 wt % filler loading). The fact that the advantage of the iPP/C_{11}-MWCNT nanocomposites in modulus over iPP/MWCNT materials was not actually realized can be explained by the increased disorder within the nanotube walls induced by the chemical functionalization. This disorder is expected form the the literature[35] to deteriorate intrinsic nanotube modulus that compensates for the effect of enhanced MWCNT dispersion in the nanocomposites. For the sPP-based composites, MWCNT functionalization results in considerably improved nanotube exfoliation in comparison with the initial state that leads to the superior polymer reinforcement: Young's modulus of sPP grows by ~84% (from ~380 to ~700 MPa) at 1.5 wt % C_{11}-MWCNT loading instead of ~55% increase at the same MWCNT content.

MWCNT functionalization has a dramatic effect on the tensile behavior of the iPP- and sPP-based nanocomposites. CNTs are highly anisotropic particles which form quite entangled networks in polymer matrices. These networks act as a defect sites hindering plastic flow of polymers. Thus, abrupt reduction in strain at break of highly crystalline iPP matrix takes place upon incorporating even low MWCNT amounts (0.2−0.4 wt %) (Figure 9a). This effect becomes less noticeable for the low-crystalline sPP (Figure 9c), and the respective composites retain relatively high elongations at break at much higher filler loadings. Nanotube functionalization induces considerable improvement in the tensile properties of the nanocomposites increasing polymer plasticity. The iPP/C_{11}-MWCNT nanocomposites retain plastic behavior at relatively high filler contents (Figure 9b): the critical C_{11}-MWCNT concentration corresponding to the transition from ductile to brittle failure is higher than 1.2 wt %. A similar improvement has been achieved for the sPP/C_{11}-MWCNT materials (Figure 9d). This effect is obviously connected with the improved nanotube dispersion caused by the attachment of alkyl chains and the reduction of entanglements between the modified MWCNTs.

Despite the noticeable transformation in the iPP/C_{11}-MWCNT nanocomposite fracture behavior in comparison with iPP/MWCNT observed by SEM, the yield strength values of the materials do not show evident improvement in the interfacial adhesion as a result of nanotube functionalization (Figure 10a,b). However, at high filler contents this yielding behavior indicates certain compatibilization achieved between the modified MWCNTs and iPP matrix. At the same time, sPP-based composites clearly demonstrate enhancement of the polymer/nanotube interaction level (Figure 10c,d) induced by MWCNT functionalization. Yield strength of sPP grows by ~17% (from 19.0 to 22.3 MPa) upon incorporating 1.5 wt % of C_{11}-MWCNTs, but at the same MWCNT content this parameter becomes improved only by ~7%. Nevertheless, the observed interfacial adhesion level remains insufficient for the efficient polymer reinforcement, and it is less than originally expected for the nanocomposites containing alkyl-functionalized CNTs. New ways of optimizing composite interfaces are needed for polypropylene.

The ultimate tensile strength of the iPP/MWCNT and iPP/C_{11}-MWCNT nanocomposites is nearly independent of nanotube loading and remains at a 31 ± 2 MPa level which testifies efficient nanotube distribution in polymer matrix, but insignificant improvement in this parameter (only by 5−7%) for iPP upon incorporating 0.1−0.4 wt % of C_{11}-MWCNTs also demonstrates limited load transfer between the polymer matrix and modified nanotubes. For the sPP-based composites, minor strengthening (about 7−8%) also takes place at low MWCNT and C_{11}-MWCNT concentrations (0.1−0.5 wt %), but higher filler loadings lead to the notable decrease in strength at break (Figure 11). This mechanical response signifies that the big nanotube aggregates detected in sPP/MWCNT composites act as stress concentrators, and the decrease of MWCNT aggregate size induced by the chemical functionalization results in the enhancement of the composite tensile strength.

Conclusion

The MWCNT chemical functionalization via attachment of $-(CH_2)_{10}CH_3$ alkyl chains as the most feasible and promising approach to the optimizing PP/MWCNT nanocomposite properties has been investigated. This method shows high efficiency in achieving better nanotube dispersion and obtaining nanocomposites combining enhanced stiffness and considerably improved plasticity that was not attainable by utilizing nonmodified MWCNTs. However, the reported results demonstrate that the great problem of creating strong interfaces between nonpolar polyolefin matrices and carbon nanotubes still remains unsolved. New efforts are required for improving nanocomposite mechanical properties by enhancing polymer−nanotube interfacial interactions. Here the most promising strategy is the incorporation of polar functional groups in PP macromolecules (for example, by propylene/methyl methacrylate block copolymerization[36]) that will apparently induce stronger interfacial interactions between polymer chains and filler particles.

Acknowledgment. The authors gratefully thank Dr. Anastasia Bolshakova and Dr. Sergey Abramchuk from Moscow State University for the assistance in electron microscopy observations, Dr. Vadim Krasheninnikov from N.N. Semenov Institute of Chemical Physics for the TGA studies of MWCNTs, and Professor Dmitry Lemenovsky from Department of Chemistry of Moscow State University for the provision of the catalyst. This work was supported by a Haldor Topsoe A/S grant.

Supporting Information Available: Raman spectra of purified and functionalized MWCNTs (Figure S1), TEM images of iPP/0.9 wt % MWCNT nanocomposite (Figure S2) and of iPP/1.2 wt % C_{11}-MWCNT nanocomposite (Figure S3), and additional SEM images of the nanocomposites (Figures S4−S6). This material is available free of charge via the Internet at http://pubs.acs.org.

References and Notes

(1) Galli, P.; Vecellio, G. *J. Polym. Sci., Part A: Polym. Chem.* **2004**, *42*, 396–415.
(2) Balow, M. J. In *Handbook of Polypropylene and Polypropylene Composites*; Karian, G. H., Ed.; CRC Press: New York, 2003; pp 1−10.
(3) Velasco-Santos, C.; Martinez-Hernandez, A. L.; Castano, V. M. *Compos. Interfaces* **2005**, *11*, 567–586.
(4) Moniruzzaman, M.; Winey, K. I. *Macromolecules* **2006**, *39*, 5194–5205.
(5) Ajayan, P. M.; Tour, J. M. *Nature (London)* **2007**, *447*, 1067.
(6) Shaffer, M. S. P.; Sandler, J. K. W. In *Processing and Properties of Nanocomposites*; Advani, S. G., Ed.; World Scientific Publishing: Singapore, 2007; pp 1−59.
(7) Schmidt, R. H.; Kinloch, I. A.; Burgess, A. N.; Windle, A. H. *Langmuir* **2007**, *23*, 5707–5712.
(8) Wiemann, K.; Kaminsky, W.; Gojny, F. H.; Schulte, K. *Macromol. Chem. Phys.* **2005**, *206*, 1472–1478.
(9) Kaminsky, W.; Wiemann, K. *Compos. Interfaces* **2006**, *13*, 365–375.
(10) Kaminsky, W.; Funck, A.; Wiemann, K. *Macromol. Symp.* **2006**, *239*, 1–6.
(11) Funck, A.; Kaminsky, W. *Compos. Sci. Technol.* **2007**, *67*, 906–915.
(12) Bonduel, D.; Bredeau, S.; Alexandre, M.; Monteverde, F.; Dubois, P. *J. Mater. Chem.* **2007**, *17*, 2359–2366.
(13) Bredeau, S.; Boggioni, L.; Bertini, F.; Tritto, I.; Monteverde, F.; Alexandre, M.; Dubois, P. *Macromol. Rapid Commun.* **2007**, *28*, 822–827.
(14) Kaminsky, W.; Funck, A. *Macromol. Symp.* **2007**, *260*, 1–8.
(15) Kaminsky, W. *Macromol. Chem. Phys.* **2008**, *209*, 459–466.
(16) Coates, G. W. *J. Chem. Soc., Dalton Trans.* **2002**, 467–475.
(17) Resconi, L.; Cavallo, L.; Fait, A.; Piemontesi, F. *Chem. Rev.* **2000**, *100*, 1253–1345.
(18) Koval'chuk, A. A.; Shchegolikhin, A. N.; Shevchenko, V. G.; Nedorezova, P. M.; Klyamkina, A. N.; Aladyshev, A. M. *Macromolecules* **2008**, *41*, 3149–3156.
(19) Mitchell, C. A.; Bahr, J. L.; Arepalli, S.; Tour, J. M.; Krishnamoorti, R. *Macromolecules* **2002**, *35*, 8825–8830.
(20) Dyke, C. A.; Tour, J. M. *J. Phys. Chem. A* **2004**, *108*, 11151–11159.
(21) Blake, R.; Gun'ko, Y. K.; Coleman, J.; Cadek, M.; Fonseca, A.; Nagy, J. B.; Blau, W. J. *J. Am. Chem. Soc.* **2004**, *126*, 10226–10227.
(22) Tasis, D.; Tagmatarchis, N.; Bianco, A.; Prato, M. *Chem. Rev.* **2006**, *106*, 1105–1136.
(23) Xu, D.; Wang, Z. *Polymer* **2008**, *49*, 330–338.
(24) Umek, P.; Seo, J. W.; Hernadi, K.; Mrzel, A.; Pechy, P.; Mihailovic, D. D.; Forro, L. *Chem. Mater.* **2003**, *15*, 4751–4755.
(25) Razavi, A.; Atwood, J. L. *J. Organomet. Chem.* **1993**, *459*, 117.
(26) Stephenson, J. J.; Sadana, A. K.; Higginbotham, A. L.; Tour, J. M. *Chem. Mater.* **2006**, *18*, 4658–4661.
(27) Xalter, R.; Halbach, T. S.; Mulhaupt, R. *Macromol. Symp.* **2006**, *236*, 145–150.
(28) Nedorezova, P. M.; Tsvetkova, V. I.; Aladyshev, A. M.; Savinov, D. V.; Klyamkina, A. N.; Optov, V. A.; Lemenovskii, D. A. *Polym. Sci., Ser. A* **2001**, *43*, 356–365.
(29) Nedorezova, P. M.; Shevchenko, V. G.; Shchegolikhin, A. N.; Tsvetkova, V. I.; Korolev; Yu, M. *Polym. Sci., Ser. A* **2004**, *46*, 242–249.
(30) McNally, T.; Potschke, P.; Halley, P.; Murphy, M.; Martin, D.; Bell, S. E. J.; Brennan, G. P.; Bein, D.; Lemoine, P.; Quinn, J. P. *Polymer* **2005**, *46*, 8222–8232.
(31) Zhou, Z.; Wang, S.; Zhang, Y.; Zhang, Y. *J. Appl. Polym. Sci.* **2006**, *102*, 4823–4830.
(32) Liang, G.; Tjong, S. C. *Adv. Eng. Mater.* **2007**, *9*, 1014–1017.
(33) Ponomarenko, A.; Shevchenko, V.; Figovsky, O. L. *Sci Isr.−Technol. Advantages* **2005**, *7*, 37–52.
(34) Thomassin, J.-M.; Pagnoulle, C.; Bednarz, L.; Huynen, I.; Jerome, R.; Detrembleur, C. *J. Mater. Chem.* **2008**, *18*, 792–796.
(35) Salvetat, J.-P.; Bonard, J.-M.; Thomson, N. H.; Kulik, A. J.; Forro, L.; Benoit, W.; Zuppiroli, L. *Appl. Phys. A: Mater. Sci. Process.* **1999**, *69*, 255–260.
(36) Jin, J.; Chen, E. Y.-X. *Macromol. Chem. Phys.* **2002**, *203*, 2329–2333.

MA801599Q